Mass Spectrometric Observation of Electron and Proton Transfer Reactions between Positive Ions and Neutral Molecules*

By A. Henglein and G. A. Muccini

Radiation Research Laboratories, Mellon Institute, Pittsburgh, Pa., U.S.A.
and Hahn-Meitner-Institut für Kernforschung, Berlin-Wannsee

(Z. Naturforschg. **17 a**, 452—460 [1962]; eingegangen am 16. März 1962)

The method of Cermak and Herman has been applied to mass spectrometric studies of symmetrical electron and proton transfer processes. The characteristics of the ion source used have been investigated both experimentally and theoretically. A new type of ionization efficiency curve is obtained if the current of a secondary ion is plotted as a function of the voltage between ionization chamber and electron trap at constant low voltage between the filament and the chamber. Essentially complete discrimination of primary ions has been achieved.

Electron transfer occurs with rather low cross section in methane but increases with molecular size and with increasing unsaturation. Large cross sections were observed in sulfur and iodine containing compounds. Double charge transfer reactions such as

$$NO^{++}+NO \rightarrow NO+NO^{++}, \qquad Xe^{++}+Xe \rightarrow Xe+Xe^{++}$$

have also been observed. Proton transfer reactions have been observed in several simple molecules. Some experimental results are presented which indicate that proton transfer may occur via a complex (at low kinetic energies) or as a stripping process (at higher energies).

Fragment ions have also been observed in the secondary mass spectra of several compounds. While part of these may result from the scattering of primary fragment ions, in some cases additional processes have to be postulated such as hydride ion transfer and dissociative charge transfer from vibrationally excited ions.

A simple new method for mass spectrometric studies of the interactions between ions and neutral molecules has recently been described by Cermak and Herman [1]. The electron accelerating voltage between the filament and the ionization chamber of a conventional ion source is kept below the ionization potential of the gas. The electrons traverse the chamber without causing any ionization and are then further accelerated by an electric field between the ionization chamber and the electron trap. The primary ions are accelerated in the direction opposite to the electron beam by this field before entering the ionization chamber. These primary ions are not able to pass the slit system of the mass spectrometer because of a kinetic energy component perpendicular to the direction of analysis. However, secondary ions produced by collisions with gas molecules in the chamber can be extracted into the analyzing section of the instrument if they are formed with negligible amounts of kinetic energy. Cermak and Herman demonstrated this in studies of dissociative charge transfer reactions in cases in which the transfer of mass and therefore of kinetic energy is extremely small.

The methodology of Cermak and Herman has been applied in studies carried out with a Consolidated Electrodynamics Corporation Model 21-103 C mass spectrometer. The sensitivity of the instrument was increased by using a Model 31 Cary (Vibrating Reed) Electrometer for the measurement of the ion currents. Studies of the characteristics of the ion source showed that essentially complete discrimination between primary and secondary ions is obtained. As a result it has been possible to investigate a number of typical resonant charge transfer reactions. In addition, the mass spectra of secondary ions of several simple compounds have been studied. It has been found that these secondary mass spectra contain not only the parent ions (formed by resonant charge transfer) but also protonated molecules as well as ions of lower masses resulting from ion-molecule reactions. It seems noteworthy to emphasize that the high degree of discrimination of primary ions makes it possible to detect certain secondary ions which cannot be observed in the conventional operation of the ion source.

* This work was supported, in part, by the U.S. Atomic Energy Commission.

[1] V. Cermak and Z. Herman, Nucleonics **19**, No. 9, 106 [1961].

Characteristics of the ion source

a) Experimental

The normal operation of the ion source is demonstrated in Fig. 1 for methane (curve 1). The current of the parent ion is given as a function of the electron accelerating voltage at constant trap voltage. A small current which decreases rapidly with decreasing electron voltage can still be observed below the ionization potential of methane (13.0 volts). Between 11.0 and 13.0 volts this current is attributed to the energy spread of the electron beam. At 11.0 volts the slope of curve 1 changes discontinuously and at lower voltages becomes nearly independent on the electron accelerating voltage. Fig. 2 shows the dependence of the CH_4^+-current on the pressure in the gas inlet system. Proportionality exists if the ion source is operated in the conventional way, i. e. with incident electron energies above the ionization potential of the methane (curve 1). The current increases with the square of the pressure if the electron accelerating voltage is kept below 11.0 volts (curve 2). In this range only secondary CH_4^+ ions which result from some interaction of primary ions formed between the chamber and trap with gas molecules in the chamber are observed.

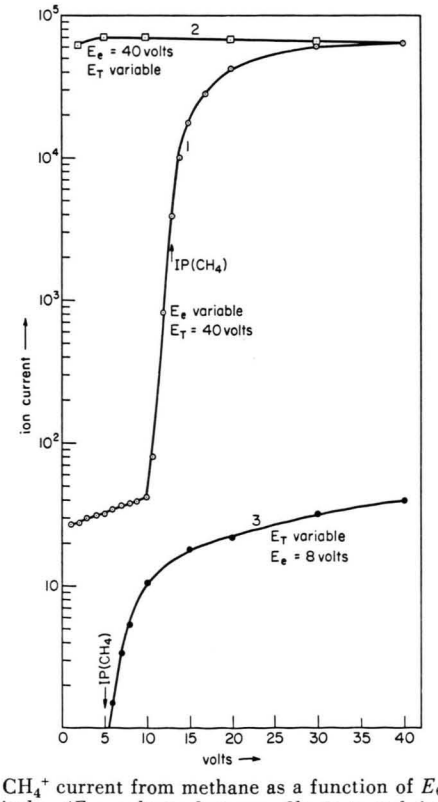

Fig. 1. CH_4^+ current from methane as a function of E_e or E_T, respectively. (E_e: voltage between filament and ionization chamber. E_T: voltage between ionization chamber and electron trap. Methane pressure in the gas inlet system: 600 μ. Repeller field: 3.8 volts/cm.)

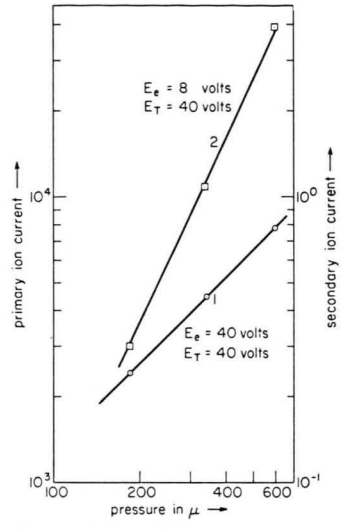

Fig. 2. Dependence of the CH_4^+ current on the pressure of methane in the gas inlet system (Curve 1: left ordinate scale, curve 2: right scale).

The formation of these secondary CH_4^+ ions is described in a more detailed manner by curve 3 in Fig. 1. The electron accelerating voltage E_e has been kept constant at 8.0 volts and the CH_4^+ current has been studied as a function of the trap voltage E_T. Curve 3 represents an "ionization efficiency curve" for the secondary ion. The "appearance potential" here amounts to 5.0 volts. This corresponds exactly to the ionization potential of 13.0 volts of methane since the energy of the electrons is equal to

$$E_e + E_T = 13.0$$

when they reach the electron trap. It can therefore be concluded that the precursor of the secondary CH_4^+ ion is the primary CH_4^+ ion which transfers its charge in a collision with a methane molecule. "Secondary ionization efficiency curves" are therefore helpful in investigations of the nature of the primary ion. However, the meaning of such secondary ionization efficiency curves is somewhat different from that obtained in more conventional ion sources. This will be discussed in detail in the following theoretical part.

The description of the characteristics of the ion source is completed by curve 2 in Fig. 1 where the

ion current is plotted versus the trap voltage at constant accelerating voltage above the ionization potential of the gas. As it is well known from conventional operation the ion current is practically independent on E_T over a wide range.

b) Theoretical

The secondary ions cannot reach the collector if they have excessive kinetic energy either parallel to the long axis of the slits (i. e. in the direction of the primary ions) or perpendicular to this axis and to the direction of analysis. Only a beam within the divergence angles α and β (perpendicular to and in the plane of analysis, respectively) will pass through the whole slit system. The angle α is determined by the length l_1 of the exit slit of the ionization chamber and l_2 of the entrance slit of the collector system as well as the distance a between the two slits. The angle β is determined by the widths d_1 and d_2 of the exit slit of the ionization chamber and the exit slit of the ion accelerating system as well as their distance b. In the mass spectrometer employed here l_1, l_2 and a were 1.0, 1.26 and 40 cm, and d_1, d_2 and b were 0.15, 0.15 and 7.2 mm, respectively. The values of α and β are calculated to be equal to 0.056 and 0.0415 radians from these data. The maximum kinetic energy components U_α and U_β parallel and perpendicular to the direction of the primary ion beam which will allow analysis are given by

$$U_\alpha = \alpha^2 V, \qquad U_\beta = \tfrac{1}{4}\beta^2 V \qquad (1), (2)$$

where V is the ion accelerating high voltage of the ion source. In this work V was equal to 800 volts. U_α and U_β are found to amount to

$$U_\alpha = 2.5 \text{ eV}, \qquad U_\beta = 0.34 \text{ eV}. \qquad (3), (4)$$

Let x_0 be the distance between the ionization chamber and electron trap, x the distance between the chamber and a point between these two electrodes. The total kinetic energy of an electron which ionizes a molecule at this point is equal to

$$E_{tot} = E_e + U(x)$$

where U is the potential difference between the chamber and this point. If the field gradient between chamber and trap is linear $U = E_T\, x/x_0$. The primary ion formed at the distance x is accelerated by the potential U and enters the chamber with the kinetic energy $e\,U(x)$. At the appearance potential, AP, of the secondary ionization efficiency curve, all ionizations take place immediately in front of the collector, i. e. $x = x_0$ and $E_{tot} = E_e + E_T$, and all primary ions entering the ionization chamber have the kinetic energy $e\,E_T$. However, at higher values of E_T ionization can occur between x_0 and a minimum distance x_1 which is given by the condition $E_e + U(x_1) = AP$. The primary ion beam therefore will have a distribution in kinetic energy between $e\,U(x_1)$ and $e\,E_T$. Since x_1 decreases with increasing E_T this distribution will become broader and broader.

The number of primary ions which are formed between x and $x + \mathrm{d}x$ (or U and $U + \mathrm{d}U$) and which will therefore obtain the kinetic energy $e\,U$ is equal to

$$N(U)\ \mathrm{d}U \propto c\ \sigma(U)\ \mathrm{d}x \qquad (5)$$

where c is the concentration of gas molecules in the ion sources and $\sigma(U)$ the cross section for ionization at the distance x, i. e. at total electron energy $E_e + U$. If $U = E_T(x/x_0)$

$$N(U)\ \mathrm{d}U \propto c(x_0/E_T)\ \sigma(U)\ \mathrm{d}U\,. \qquad (6)$$

The total number of primary ions formed between x_0 and x_1 will amount to

$$N_{tot} \propto c(x_0/E_T) \int_{AP-E_e}^{E_T} \sigma(U)\ \mathrm{d}U\,, \qquad (7)$$

$\sigma(U)$ is easily derived from the conventional ionization efficiency curve. For example, curve 1 in Fig. 3 represents $\sigma(U)$ for CH_4^+ if E_e is equal to 8 volts.

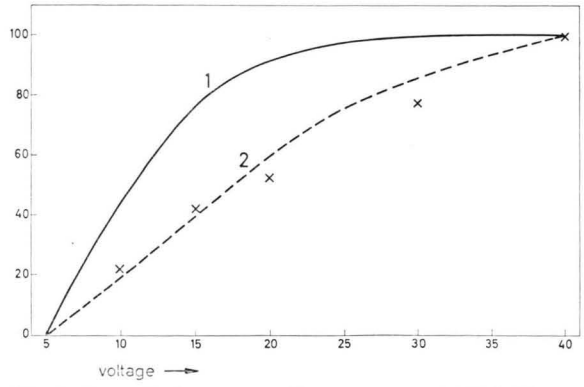

Fig. 3. Curve 1: Ionization efficiency curve of CH_4^+ (E_T constant at 40 volts. E_e variable. Abscissa: $E_e - 8$ volts. Curve 1 is normaziled at $E_e - 8 = 40$ volts). Curve 2: Total primary CH_4^+ current as function of E_T at E_e = constant at 8 volts. (Curve 2 is calculated from curve 1 according to Eq. (7). Normalization of curve 2 at $E_T = 40$ volts). X: Observed secondary CH_4^+ current at various values of E_T (E_e constant at 8 volts. Normalization at $E_T = 40$ volts).

This curve is the measured primary ionization efficiency curve 1 in Fig. 1 (the scale of the abscissa is just shifted by 8 volts). Curve 2 in Fig. 3 is the integral

$$(1/E_T) \cdot \int_{AP-8}^{E_T} \sigma(U)\, dU$$

of curve 1 and represents the total primary CH_4^+ current at different voltages E_T. Both curves are normalized at 40 volts.

The number of secondary ions which are produced by reactions of the primary ions in the ionization chamber is proportional to

$$N'_{tot} \propto c \int_{AP-E_e}^{E_T} N(U)\, \sigma'(U)\, dU \qquad (8)$$

where $\sigma'(U)$ is the cross section of the ion-molecule reaction. By combining Eq. (6) and (8)

$$N'_{tot} \propto c^2 (x_0/E_T) \int_{AP-E_e}^{E_T} \sigma(U)\, \sigma'(U)\, dU \qquad (9)$$

is obtained. If σ' is independent of the kinetic energy of the primary ion, N'_{tot} becomes proportional to N_{tot}, i. e. the shape of the secondary ionization efficiency curve will be identical to that calculated from Eq. (7) (Fig. 3). In these considerations it has been assumed that all secondary ions reach the collector. However, if the secondary ions are formed with kinetic energies perpendicular to the direction of flight only a fraction, f, will be collected. As the kinetic energy of the primary ion increases f will decrease and N' will be described by the relation

$$N'_{tot}(E_T) \propto c^2 (x_0/E_T) \int_{AP-E_e}^{E_T} \sigma(U)\, \sigma'(U)\, f(U)\, dU \qquad (10)$$

Symmetrical charge transfer reactions

Symmetrical charge transfer processes have been studied by a number of authors [2–5]. These investigations have mainly been restricted to the noble gases. The reaction $H_2^+ + H_2 \rightarrow H_2 + H_2^+$ seems to be the only process studied in which molecular species are involved. The cross sections of such resonance processes are expected and have been found to be higher than gas collision cross sections. This arises because the resonance introduces a long range interaction which would otherwise not occur. Relatively little variation of the cross section with the kinetic energy of the ion has been found. At energies above 200 eV in all cases the cross section observed falls very slowly and steadily as the relative kinetic energy of the collision partners increases. At lower kinetic energies, however, a small maximum has been observed in argon and in neon [6] and a very pronounced one in hydrogen [4]. These anomalies have been attributed to the occurrence of non-resonant processes in the noble gases due to the spin multiplicity of the lowest state of these ions. In the case of H_2 a side reaction in which a change of vibrational energy is involved has been assumed [4]. Scattering of ions in the case of exact resonance occurs primarily at small angles, the scattering intensity at 90° being practically zero [7]. It can therefore be assumed that all secondary parent ions formed in our ion source exclusively result from symmetrical charge transfer.

Fig. 3 contains a few points from curve 3 in Fig. 1. These points fit curve 2 in Fig. 3 fairly well. This curve is calculated on the assumption that both $f(U)$ and $\sigma'(U)$ in Eq. (10) are constant over the range from 5 – 40 volts. The agreement indicates, as mentioned above, that the transfer of kinetic energy is very small and that the cross section of the observed process is not significantly dependent on the kinetic energy.

Fig. 4 shows the ionization efficiency curves for the secondary ions observed in methane and Figs. 5 – 7 show similar data for some other simple molecules. The appearance potentials of the parent ions are always identical with those of the primary parent ions. All observed symmetrical charge transfer processes are listed in Table 1. The lowest cross section for transfer of a single electron has been found in methane. This reaction has been selected for reference in Table 1. In order to obtain relative cross sections, the ratio

$$\frac{\text{current of secondary ion at } E_e = 8 \text{ and } E_T = 40 \text{ volts}}{\text{current of primary ion at } E_e = 40 \text{ and } E_T = 40 \text{ volts}} \qquad (11)$$

has been measured relative to the similar ratio for methane. This procedure assumes that the primary ion current in the CERMAK–HERMAN operation of the ion source ($E_e = 8$, $E_T = 40$) is proportional to the

[2] H. S. W. MASSEY and E. H. S. BURHOP, Electronic and Ionic Impact Phenomena, Clarendon Press, Oxford 1952, p. 525.
[3] J. B. HASTED, Proc. Roy. Soc., Lond. A **205**, 421 [1951].
[4] H. B. GILBODY and J. B. HASTED, Proc. Roy. Soc., Lond. A **238**, 334 [1956].
[5] J. B. HASTED, Adv. in Electronics and Electron Phys. **13**, 1 [1960].
[6] A. ROSTAGNI, Nuovo Cim. **12**, 134 [1935].
[7] Reference [2], p. 443.

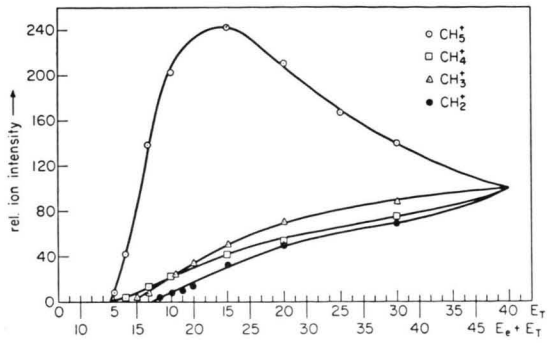

Fig. 4. Ionization efficiency curves of secondary ions in methane (E_e=constant at 8 volts. E_T variable. All curves normalized at E_T=40 volts).

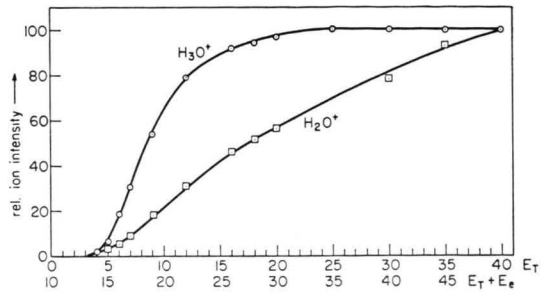

Fig. 5. Ionization efficiency curves of secondary ions in water (E_e=constant at 10 volts. E_T variable).

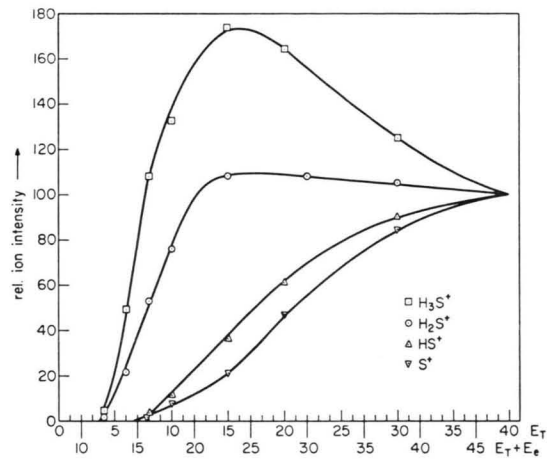

Fig. 6. Ionization efficiency curves of secondary ions in hydrogen sulfide (E_e=8 volts, E_T variable).

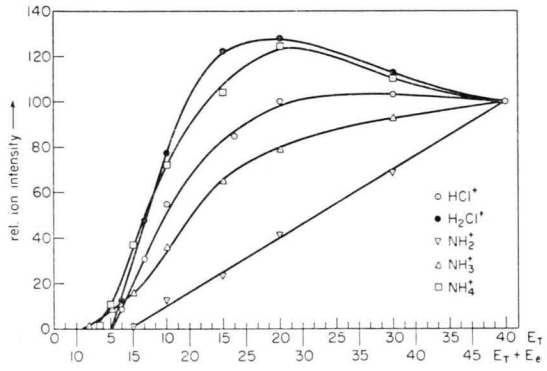

Fig. 7. Ionization efficiency curves of secondary ions in hydrogen chloride and ammonia (E_e=8 volts, E_T variable).

ion	relative cross section	ion	relative cross section
CH_4^+[a]	(1.0)[a]	HCl^+	7.0
$C_2H_6^+$	3.3	NH_3^+	7.8
$C_2H_4^+$	10	H_2S^+	15
$C_2H_2^+$	14	CS_2^+	19
c-$C_6H_{12}^+$	5.0	I_2^+	27
c-$C_6H_{10}^+$	29	Ne^+	3.7
$C_6H_6^+$	13	Ar^+	9.3
NO^+	4.1	Kr^+	15
H_2O^+	4.2	Xe^+	23
CO_2^+	4.3		
Ar^{++}	1.1		
Kr^{++}	1.8		
Xe^{++}	3.0		
NO^{++}	0.3		

[a] Reference reaction: $CH_4^+ + CH_4 \rightarrow CH_4 + CH_4^+$

Table 1. Relative cross section of symmetrical charge transfer reactions.

ion current in the more conventional operation of the source (i. e. $E_e = 40$ volts). Since the primary ion current contained ions of kinetic energies between about 5 and 40 volts, the value of the cross section obtained is an average over this range. An additional complication arises since the primary molecular ions formed by electron impact will have various amounts of vibrational energy. The data obtained by the present method of measuring cross sections can be compared with literature values in the case of the noble gases. Our ratio of the cross sections in argon and neon amounts to $9.3/3.7 = 2.5$ which agrees with the ratio of $2.5 - 3.0$ calculated from the measurements of ROSTAGNI [6]. Absolute cross sections may be calculated from the data in Table 1 by using the known absolute cross section of the transfer process in argon (38×10^{-16} cm^2 at 20 eV).

The cross section depends significantly on the nature of the compound. In molecules of similar size (such as ethane, ethylene and acetylene) the cross section increases with increasing unsaturation. A similar increase is observed by going from cyclohexane to cyclohexene. High cross sections have been found in the sulfur containing compounds and in iodine. Table 1 also contains some examples of symmetrical double charge transfer. In these experiments, 110 volts were used instead of 40 to carry out the measurements and Eq. (11) adjusted accordingly. The process

$$NO^{++} + NO \rightarrow NO + NO^{++} \qquad (10)$$

was the only one found for the transfer of two charges in a molecular system.

Proton transfer reactions

The secondary mass spectra of some simple molecules are listed in Table 2. The ionization efficiency curves of these secondary ions are shown by Figs. 4 – 7. Ions of the form $H_{n+1}X^+$ from parent molecules H_nX have been observed in all cases. The secondary ionization efficiency curves of these ions begin at the same appearance potentials as those of the parent ions H_nX^+. Primary ions H_nX^+ must there-

Substance[a]	Ion	ionization potential (volts)[c]	relative intensity	
			primary spectrum[b]	secondary spectrum[b]
water	H_3O^+		2.4	29
	H_2O^+	12.61	100	100
	OH^+	~ 12.8	20	—
	O^+	13.61	0.7	—
hydrogen sulfide	H_3S^+		<0.04	2
	H_2S^+	10.47	100	100
	HS^+		38	4
	S^+	10.36	41	3
hydrogen chloride	H_2Cl^+		1.2	7
	HCl^+	12.90	100	100
	Cl^+	13.01	15	0.7
ammonia	NH^+_4		0.6	15
	NH^+_3	10.52 — 11.3	100	100
	NH^+_2		67	2
	NH^+		3.5	—
	N^+	14.54	7.8	—
methane	CH^+_5		2.8	20
	CH^+_4	13.1	100	100
	CH^+_3	9.9	78	120
	CH^+_2	11.9	12	6
	CH^+	11.13	5	—
	C^+		1	—
ethane	$C_2H^+_7$		not detectable	0.2
	$C_2H^+_6$	11.6	100	100
	$C_2H^+_5$	8.7	82	122
	$C_2H^+_4$	10.51	410	93
	$C_2H^+_3$		133	17
	$C_2H^+_2$	11.41	74	3
	C_2H^+		6	—
	C_2^+		0.8	—
ethylene	$C_2H^+_5$		not detectable	2
	$C_2H^+_4$	10.51	100	100
	$C_2H^+_3$		54	9
	$C_2H^+_2$	11.41	52	5
	C_2H^+		8	—
	C_2^+		1	—

[a] Pressure of the gas inlet system: 600 μ. Repeller field: 3.84 volts/cm.
[b] Primary spectra: $E_e = 40$ volts, $E_T = 40$ volts. Secondary spectra: $E_e = 8$ volts, $E_T = 40$ volts.
[c] Data taken from F. H. Field and J. L. Franklin, Electron Impact Phenomena, Academic Press Inc., New York 1957.

Table 2. Primary and secondary mass spectra of simple molecules.

fore be the precursors of the protonated species as well as the secondary parent ions.

$$H_nX^+ + H_nX \begin{cases} \nearrow H_nX + H_nX^+ & (13) \\ \searrow H_{n-1}X + H_{n+1}X^+ & (14) \end{cases}$$

In order to compare the competing processes of electron and proton transfer the ratio of the currents of the secondary ions $H_{n+1}X^+$ and H_nX^+ is plotted in Fig. 8 versus the voltage E_T.

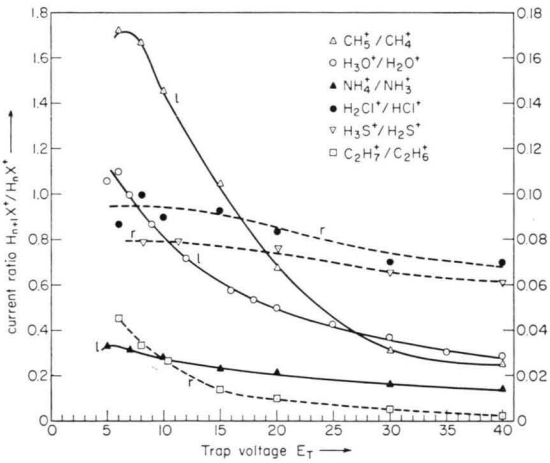

Fig. 8. Current ratio of protonated molecules and secondary parent ions as a function of E_T (E_e=8 volts. l and r: left and rigth ordinate scale, respectively).

The general shape of the secondary ionization efficiency curves of the ions $H_{n+1}X^+$ differs markedly from that of the ions X_nX^+. A maximum at 10 – 15 volts above the appearance potential can usually be observed (Figs. 4 – 7). The decrease in the ratio $H_{n+1}X^+/H_nX^+$ in Fig. 8 indicates that electron transfer predominates more and more at higher kinetic energies. The shape of the $H_{n+1}X^+$ curves in Figs. 4 – 7 may be explained by the inverse dependencies of σ, σ' and f on the kinetic energy eU of the primary ions [Eq. (10)]. The increase in $\sigma(U)$ at rather low kinetic energies determines the main features of the shape of the curve while the decrease in $\sigma'(U)$ and in $f(U)$ becomes predominant at higher kinetic energies. The decrease of σ' is well known from conventional studies on ion-molecule reactions [8, 9]. It may be described by the relation

$$\sigma' \propto U^a \qquad (15)$$

over a certatin range of U. Values for a of -0.5 to -1.4 have been observed for different reactions [10].

The collection efficiency, $f(U)$, can no longer be assumed to be constant as in the electron transfer reactions since the transfer of the mass of the proton will be accompanied by the transfer of kinetic energy. This term is therefore expected to decrease above a certain value of U, but the decrease should depend strongly on the nature of the collision. The reaction may occur via an activated complex which dissociates into the final products after a lifetime much longer than the time of a molecular vibration. The existence of such complexes has been proven indirectly [9] and directly [11, 12] in several ion-molecule reactions. Complexes are probably preferentially formed at low kinetic energies. At higher kinetic energies the lifetime of the complex will become shorter than the time required for distribution of the excitation energy in the various degrees of freedom in the complex, i. e. there is practically no real complex formation. Reactions which are observed at higher kinetic energies are more likely to occur as stripping processes. Essentially the cross sections of such processes are not expected to exceed gas kinetic cross sections. In the case of complex formation the intermediate complex will move with half the original kinetic energy (eU) in the direction of the primary ion, the rest of the kinetic energy appearing as internal energy. The reaction product $H_{n+1}X^+$ will have the kinetic energy

$$\tfrac{1}{2}(eU)[(A+1)/(2A)] \sim \tfrac{1}{4}(eU) \qquad (16)$$

in the direction of the primary ion (where A is the mass of molecule H_nX). It will have an additional component of kinetic energy directed at random if part of the excitation energy of the complex and of the exothermicity of the reaction appears as kinetic energy of the final products. At values of U above 10 volts the maximum energy component U_a, at which collection is allowed, will have been reached. The collection efficiency is expected to fall significantly as the kinetic energy of the primary ion exceeds a few electron volts.

Where the secondary ion results from stripping of a proton from the primary ion the protonated molecule will be formed with the kinetic energy

[8] D. P. Stevenson and D. O. Schissler, J. Chem. Phys. **29**, 282 [1958].
[9] F. H. Field, J. L. Franklin and F. W. Lampe, J. Amer. Chem. Soc. **79**, 2419 [1957].
[10] A. Henglein, Z. Naturforschg. **17 a**, 37 [1962].
[11] R. F. Pottie and W. H. Hamill, J. Phys. Chem. **63**, 877 [1959].
[12] A. Henglein, Z. Naturforschg. **17 a**, 44 [1962].

$A^{-1}(A+1)^{-1}(eU)$ in the direction of the primary ion. This amount is much less than in the case of complex formation. There $f(U)$ is expected to depend only slightly on the kinetic energy in the range of $5-40$ volts. The ratio $H_{n+1}X^+/H_nX^+$ in Fig. 8 is only slightly dependent on E_T in the cases of hydrogen chloride, hydrogen sulfide and ammonia. If we can again assume that σ' and f of the electron transfer are nearly independent on energy it must be concluded that σ' and f of the proton transfer show the same behavior. The stripping model would therefore be more adequate to describe these reactions than the activated complex model (at least for kinetic energies above 5 eV). The very strong decrease in the current ratio CH_5^+/CH_4^+ in Fig. 8 indicates that this reaction occurs via a complex at low kinetic energies while a stripping reaction predominates at higher energies. This may also explain some observations of FIELD et al.[9] who studied the reaction $CH_4^+ + CH_4 \rightarrow CH_5^+ + CH_3$ by operating the ion source in the conventional way. They found the cross section to decrease at repeller field strengths between $10-100$ volts/cm but to become constant at higher field strengths.

The $C_2H_7^+$ ion which could not be detected in conventional studies on ion-molecule reactions in ethane[13] has been observed (Table 2, Fig. 8) with low intensity. Since the appearance potentials of $C_2H_6^+$, $C_2H_5^+$ and $C_2H_4^+$ from ethane no not differ very much, it is difficult to attribute the secondary $C_2H_7^+$ to one of these primary ions. A rough estimate shows that the cross section of the formation of $C_2H_7^+$ in ethane must be 100 times smaller than that of the proton transfer in water. This low cross section explains the failure to detect $C_2H_7^+$ in the conventional operation of an ion source since $C_2H_7^+$ is here masked by the C^{13} isotopic peak of the $C_2H_6^+$ ion.

Fragment ions in the secondary mass spectra

The secondary mass spectra in Table 2 contain a number of ions of lower mass numbers. Their secondary appearance potentials are identical with the known appearance potentials of these ions when formed by electron impact. It cannot be ruled out that primary ions are not scattered and pass through the slit system of the mass spectrometer. The collection efficiency of scattered ions is expected to be very small since most will have components of kinetic energy perpendicular to the direction of analysis. Furthermore, the scattering intensity at 90° is very low[14]. This would explain the rather low relative intensities of most of the fragment ions in Table 2. The table, however, contains a few examples which strongly indicate that there must be additional processes of formation of secondary fragment ions.

The ion CH_3^+ is the most abundant in the secondary mass spectrum of methane. Its intensity is even higher than that of CH_4^+ (the abundant ion in the primary mass spectrum). Furthermore, the secondary ionization efficiency curve of CH_3^+ always runs above that of CH_4^+ except for the immediate vicinity of the appearance potential of CH_3^+ (Fig. 4). This is in contrast to the behaviour of the primary ionization efficiency curves of these ions[15]. It must be concluded that CH_3^+ ions are formed by some ion-molecule reactions such as H^- transfer from methane

$$CH_3^+ + CH_4 \rightarrow CH_4 + CH_3^+ \qquad (17)$$

or dissociative electron transfer

$$CH_4^{+*} + CH_4 \rightarrow CH_4 + CH_3^+ + H \qquad (18)$$

If reaction (18) is initiated by a CH_4^+ ion in its ground state the energy deficit $D(CH_3^+ - H)$ has to be taken from the kinetic energy of the CH_4^+ ion. The cross section of this process would be very small since the collision occurs adiabatically in the energy range studied. However, if the CH_4^+ ion is formed with an amount of vibrational energy only about one-tenth of an electron volt smaller than $D(CH_3^+ - H)$ the rest of the energy deficit may easily be delivered by the kinetic energy. It is at present not possible to distinguish between reactions (17) and (18). Similarly the $C_2H_5^+$ ion occurs with abnormally high intensity in the secondary mass spectrum of ethane. It is therefore attributed to the analogous reactions

$$C_2H_5^+ + C_2H_6 \rightarrow C_2H_6 + C_2H_5^+ \qquad (19)$$

or

$$C_2H_6^{+*} + C_2H_6 \rightarrow C_2H_6 + C_2H_5^+ + H. \qquad (20)$$

The OH^+ ion could not be detected in the secondary spectrum of water although its intensity as primary ion is very high. The absence of this ion as a

[13] F. W. LAMPE and F. H. FIELD, J. Amer. Chem. Soc. **81**, 3242 [1959].
[14] Reference [2], p. 496–497.
[15] A. HENGLEIN and G. A. MUCCINI, Z. Naturforschg. **15a**, 584 [1960].

secondary ion would seem to corroborate the above ideas that the high intensities observed for CH_3^+ and $C_2H_5^+$ cannot be due to scattering of the primary ions. It also indicates that hydride ion transfer

$$OH^+ + H_2O \rightarrow H_2O + OH^+ \qquad (21)$$

does not occur. The ionization potential of OH seems to be slightly higher than that of water while that of CH_3 is much lower than that of methane (Table 2). In the case of water electron transfer

$$OH^+ + H_2O \rightarrow OH + H_2O^+ \qquad (22)$$

is expected to compete with reaction (21). Reaction (22) is of interest in considerations of the radiation chemistry of water. It explains the fact that there is no chemical evidence of OH^+ although the mass spectrum of water indicates that OH^+ is formed in high yield by high energy radiation. In the case of hydrogen chloride, the fragment Cl also has a slightly higher ionization potential than the molecule. The reaction $Cl^+ + HCl \rightarrow Cl + HCl^+$ may therefore partly be responsible for the very low relative intensity of Cl^+ in the secondary mass spectrum of hydrogen chloride.

Isotopie-Effekt und Häufigkeiten der Edelgase in Steinmeteoriten und auf der Erde

Von J. ZÄHRINGER

Aus dem Max-Planck-Institut für Kernphysik, Heidelberg

(Z. Naturforschg. **17 a**, 460—471 [1962]; eingegangen am 2. April 1962)

The rare gas content of 19 various stone meteorites has been investigated mainly for the abundance of the heavier components. Nine normal chondrites have been selected, which indicated from the A^{36}/A^{38}-ratio the presence of primordial rare gases. All of them contain primordial Kr and Xe as well as Xe^{129}-excess. Their content is proportional to the A^{36}-content and increases in the sequence: normal chondrites, enstatite chondrites and carbonaceous chondrites.

The relative abundances of the rare gases in the Staroe Pesjanoe and Kapoeta meteorites follow very closely the SUESS-UREY abundance curve. This may indicate that their composition is very similar to that of an undifferentiated solar nebula.

The isotopic variations of meteoritic and terrestrial Ne and He can be explained by isotope dependant diffusion in solids under the assumptions, that all matter contained the rare gases in solar composition previous to degassing and that Kr and A has been lost to a much smaller extent. A similar process may be responsible for the Xe-anomalies. Heating experiments confirm, that the remaining gases are in thermally resistent components. The Xe^{129}-problem is discussed under these aspects.

Der erste sichere Nachweis von Uredelgasen in Meteoriten gelang GERLING und LEVSKII [1] in dem Achondriten Staroe Pesjanoe. Dieser Meteorit enthält große Mengen an He, Ne und A, die nicht durch radioaktiven Zerfall oder durch Spallationsprozesse entstanden sein können. Ganz ähnliche Edelgasmengen wurden später in dem Achondriten Kapoeta von ZÄHRINGER und GENTNER [2] und auch in dem Chondriten Pantar von KÖNIG et al. [3] und MERRIHUE et al. [4] festgestellt.

Neben diesen heliumreichen Meteoriten existieren andere, wo überwiegend die schweren Edelgase außergewöhnlich häufig sind. So fand REYNOLDS [5] in dem kohligen Chondriten Murray überschüssiges A, Kr und Xe, STAUFFER [6] in einigen kohligen Chondriten und einem Ureiliten kleinere Mengen A und Ne, ZÄHRINGER und GENTNER [2] und REYNOLDS [7] in Enstatitchondriten erhöhte A-, Kr- und Xe-Häufigkeiten. Inzwischen hat sich gezeigt, daß das Vorhandensein von Uredelgasen keine Ausnahme darstellt und daß unter günstigen Bedingungen in den meisten Chondriten Urargon zu erkennen ist [8].

Die Isotopenzusammensetzungen der Uredelgase sind denen der atmosphärischen Edelgase ähnlich.

[1] E. K. GERLING u. L. K. LEVSKII, Dokl. Akad. Nauk, SSSR **110**, 750 [1956].
[2] J. ZÄHRINGER u. W. GENTNER, Z. Naturforschg. **15 a**, 600 [1960].
[3] H. KÖNIG, K. KEIL, H. HINTENBERGER, F. WLOTZKA u. F. BEGEMANN, Z. Naturforschg. **16 a**, 1124 [1961].
[4] C. M. MERRIHUE, R. O. PEPIN u. J. H. REYNOLDS, J. Geophys. Res., im Druck.
[5] J. H. REYNOLDS, Phys. Rev. Letters **4**, 8 u. 351 [1960].
[6] H. STAUFFER, Geochim. Cosmochim. Acta **24**, 70 [1961].
[7] J. H. REYNOLDS, Z. Naturforschg. **15 a**, 1112 [1960].
[8] T. KIRSTEN, D. KRANKOWSKY u. J. ZÄHRINGER, Geochim. Cosmochim. Acta, im Druck.